



Egyptian Knowledge Bank



***International Journal of Advances in Structural
and Geotechnical Engineering***

<https://asge.journals.ekb.eg/>

Print ISSN 2785-9509

Online ISSN 2812-5142

Special Issue for ICASGE'19

***Numerical Modeling on Infilled RC Frames
Retrofitted with ECC Subjected to Cyclic Loads***

Mohamed A. Sakr, Saher R. El-khoriby, Tarek M. Khalifa, and Ahmed A. Badawy

ASGE Vol. 03 (03), pp. 126-141, 2019

NUMERICAL MODELING ON INFILLED RC FRAMES RETROFITTED WITH ECC SUBJECTED TO CYCLIC LOADS

**Mohamed A. Sakr¹, Saher R. El-khoriby², Tarek M. Khalifa³, and
Ahmed A. Badawy⁴**

^{1,2} Professor, Faculty of Engineering, Tanta University, Egypt

E-mail: mhsakr010@yahoo.com

E-mail: drsaher2012@yahoo.com

³lecture, Faculty of Engineering, Tanta University, Egypt.

⁴ Assistant lecturer, Faculty of Engineering, Tanta University, Egypt.

E-mail: eng.ahmedali22@yahoo.com

ABSTRACT

Masonry-infilled reinforced concrete (RC) frames constitute a significant part of the building inventory in earthquake-prone regions around the world, only a relatively small number of experimental studies have been performed in order to examine the impact of a thin layer of Engineered Cementitious Composites (ECC) for retrofitting infilled panel of RC- frames. So, a numerical parametric study is essential.

This paper presents a nonlinear finite-element modeling method to evaluate the seismic behavior of RC infilled frames that have retrofitted with ECC, in this study, behavior of infilled RC frame has been investigated using Abaqus's standard package. The modeling was calibrated based on experimental results and then a parametric study was carried out, these parameters include the column depth, infill panel type and ECC retrofitting configurations.

The analysis included 2D model using plane stress element. Moreover, nonlinearities of the concrete, infill panel, steel and ECC have been considered.

The obtained results indicate that several important conclusions reflecting the effects of the studied ECC- retrofitting technique and the numerical modeling can predict load-displacement curves and crack propagation process with good agreement with experimental data.

Keywords: Masonry, Infill wall, ECC, Finite Element Model.

1. INTRODUCTION

Masonry infills in non-ductile reinforced concrete frames can be found in many places around the world. Masonry infills have been widely used because of their good thermal and acoustic insulation properties, for aesthetic reasons and for fire resistance. Although in design masonry infills are considered as non-structural elements, they can develop a strong interaction with the bounding frames when subjected to earthquake loads and, therefore, contribute significantly to the lateral stiffness and load resistance of the structure. Despite several decades of research, the performance of these structures in a severe earthquake remains a major controversy among structural engineers and researchers today. Improving their seismic performance using innovative techniques and materials is a promising way to address this problem.

Different retrofit techniques have been investigated by researchers and used by practitioners for unreinforced masonry walls in order to improve their performance, the most common being a single- or double-sided shotcrete jacket with welded wire steel mesh [1,2], with this method, substantial weight is added to the structure that may require upgrading the structure's foundation and therefore this method can be uneconomical. Furthermore, when a double-sided jacket is provided there is a negative impact on the aesthetics of the structure. An alternative retrofit technique has been the addition of framing elements in order to reduce the load taken by the wall [3]. However, this method also alters the aesthetics and can increase substantially the weight of the structure. The use of epoxy-bonded fiber-reinforced polymer (FRP) laminates [4] and ferrocement and plaster overlays [5] have also been investigated. FRP laminates are very effective in enhancing substantially the strength of the masonry infill. However, debonding of the FRP due to a poor preparation of the masonry surface before the application can be the controlling mechanism of failure.

A new seismic retrofit technique for unreinforced masonry infills in non-ductile reinforced concrete frames is investigated herein to prevent the soft-story phenomenon and minimize falling hazards in these structures. Enhancing the ductility and delaying the strength degradation of unreinforced masonry infills are of primary importance to achieve this goal. To that end, a sprayable ECC is investigated as an infill retrofit method. ECC belongs to a class of high-performance fiber-reinforced cement-based composites that exhibit fine, multiple cracking and a strain hardening response in direct tension. The material is micromechanically designed to achieve this response using a small volume fraction of polymeric fibers (less than 2% by volume) [6]. The fibers are randomly oriented and distributed and are typically 12-mm long while very fine sand is used with a particle size typically 110 μm in diameter. Sprayable ECC mix designs have been developed recently and were shown to be a promising repair material for deteriorated reinforced concrete structures [7].

The aim of this study is to utilize engineered cementitious composites (ECC) as a strengthening material to enhance the seismic behavior of infilled RC frames. ECCs are a special kind of high-performance fiber reinforced cement-based composite materials (HPFRCCs) which are typically reinforced with short fibers and micromechanically tailored to feature high tensile ductility and multiple cracking [8]. To utilize new repair materials ECCs have been utilized by some researchers for repairing infrastructures using wet-mix shotcreting process [9], making precast panels for retrofitting frame structures [10], and strengthening unreinforced masonry panels [11]. The experimental studies have shown that ultra-high ductility of ECC can considerably enhance the behavior of the strengthened structural system, resulting in high denomination resistance, high ductility and increased load-carrying capacity of the system. In the present study, the ECC strengthening technique which can be applied with minimum disturbance to the occupants extends to the field of retrofitting brick-infilled concrete frames [11]. In this paper the efficiency of ECC overlays is evaluated and the behavior of test specimens subjected to quasi-static cyclic lateral loading in terms of the strength, stiffness, and energy absorption capacity is discussed. Furthermore, the ideal backbone curves obtained are presented, which can be utilized in numerical simulation. Lastly, the drift limits usually considered in seismic design corresponding to initiation of significant damages are introduced. As shown in the literature many studies have reported experimentally the results and benefits of infilled frames on the seismic behavior of structures and the benefits of ECC strengthening on the infilled frames to increase their in-plane shear capacity and dissipated energy. Numerical analysis provides better insight into understanding the exact behavior of the infilled frames. This needs a validated numerical model which is calibrated by experimental results. In this paper, this study presents the results of an analysis, FE model conducted to predict the behavior of RC frame with un-retrofitted and retrofitted masonry infill with ECC under in-plane cyclic loading under.

2. FINITE ELEMENT MODLE

In order to obtain an efficient and accurate finite element model (FEM), the analysis was conducted in ABAQUS/Standard module [12]. All parts of models are presented detailed as follows and Brief descriptions of the constitutive models that are used in the model are described below. The proposed FEM validated with the experimental results proposed by Sakr et al. [13] and Kyriakides et al. [16] to specify its accuracy.

2.1 Constitutive Models

By using "concrete damage plasticity" (CDP) model for modeling the concrete, infill panel and the ECC material behavior. The compressive crushing failure and tensile cracking failure are assumed about this model [12]. The fracture energy method was used to specify the post-peak tension failure behavior of concrete, infill and ECC. For the uni-axial compression stress-strain curve of the concrete, the stress-strain relationship proposed by Saenz [15] was used as reported. The steel is modeled to be bilinear elastic-plastic material and definitions in tension and compression.

2.2 2D Analysis using plane stress element

For modeling concrete, infill panel, and ECC material at 4-node bilinear, reduced integration with hourglass control elements (CPS4R) was used. And for the reinforcement steel at 2-node linear 2-D truss (T2D2) element was used, the frame was modelled as fixed-fixed. And the interaction between the concrete and the RFT was assumed to be fully bonded modelled by the embedded region constraint.

2.3 Interaction between Concrete Frame and Infill Panel

In order to represent the interaction between the concrete frame and the infill panel surface-to-surface contact definition can be used to model contact interactions between specific two surfaces in a model, the master surface and the slave surface, the concrete frame interior surface has been used as the master surface and the infill panel exterior surface as the slave surface. And the used friction coefficient was 0.25 as recommended by [23].

2.4 Interaction between ECC material and Infill Panel

To represent the interface between ECC material and the infill panel surface, the model was constructed using node-to-node interaction method using Cartesian connector element. By using the traction separation law to allow for the debonding failure mode, **Error! Reference source not found.** The available traction-separation model assumes initially linear elastic behavior followed by the initiation and evolution of damage. This model was suggested by obidat et al. [24].used that model with values induced based on the experimental.

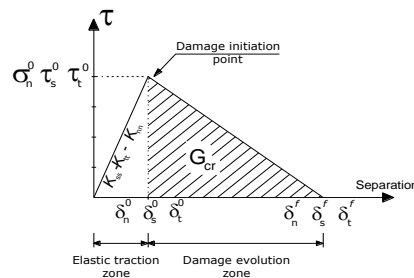


Fig. 1: Description of the traction-separation behavior, (ABAQUS)

3. VERIFICATION OF THE MODEL WITH PREVIOUS WORK

Experimental investigation of size effects is expensive as a wide range of dimensions of the similar structures need to be tested to establish a full-size effect law. For such purpose, the most versatile, cost-effective numerical simulations is often carried out.

3.1 Bare frame

To calibrate the behavior of the bare frame model, a comparison is carried out between the finite element results and that reported in the experimental work of Sakr et al. [13]. The experimental program consisted of 1/2 scale model of a single-story concrete subjected to in-plane quasi-static cyclic tests. Dimensions and RFT details of the frame is shown in Fig. 2.

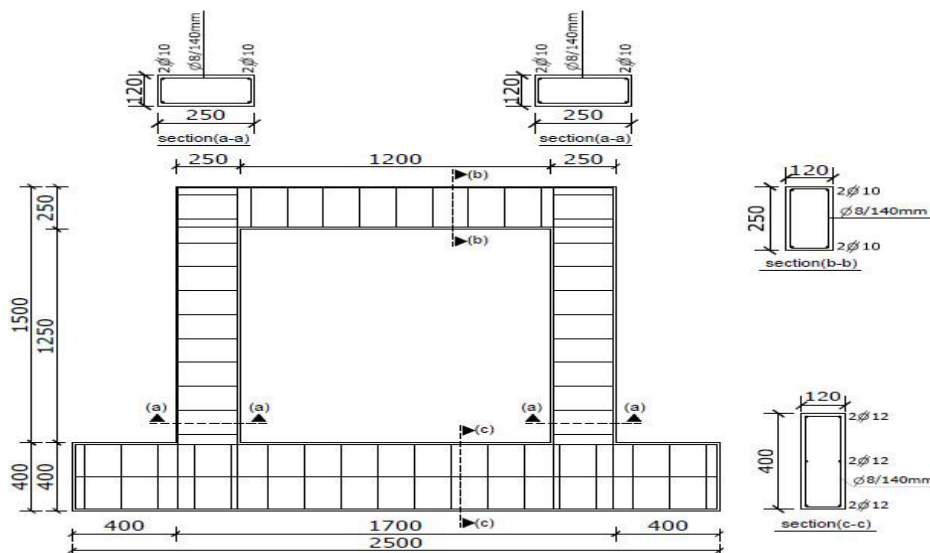


Fig. 2: Dimensions and reinforcement details of test frame Sakr et al. [13].

3.1.1 Material properties

3.1.1.1 Concrete

In the experimental study, the average compressive strength $\bar{\sigma}_c$ was in the experimental work 25 MPa. E_c and σ_{ct} were then calculated as shown in Fig. 3 the stress–strain relationship proposed by Saenz [15]. Poisson’s ratio for concrete was assumed to be 0.20.

To specify the post-peak tension failure behavior of concrete, the fracture energy method is used. The fracture energy, G_f , is the area under the softening curve. As it is usually a parameter subjected to relatively high uncertainty, and depending on the grade of concrete, the aggregate size etc. The optimum value of fracture energy was found to be equal 600J/m²[14].

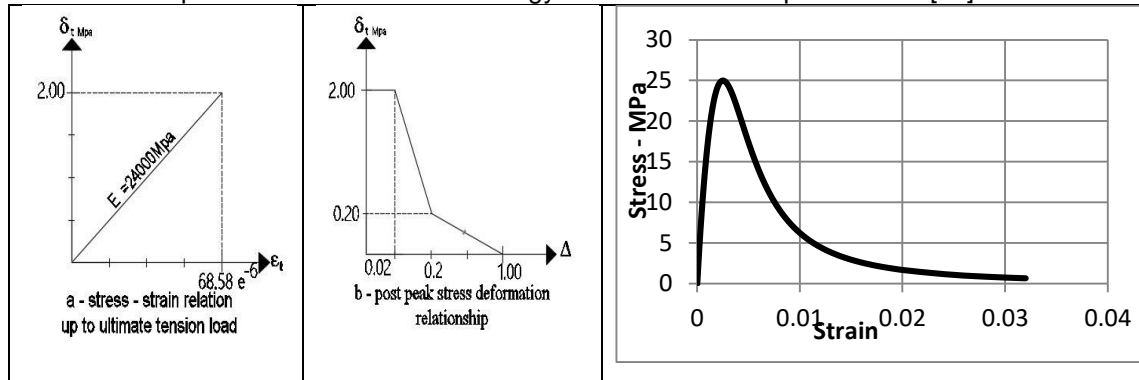


Fig. 3: Concrete material properties

3.1.1.2 Reinforcement steel

The main steel which is used in the experimental work has parameters under cyclic loading shown in Table 1 [22].

Table 1: Calibration parameters of steel

σ_0 (N/mm ²)	Q_∞ (N/mm ²)	b	C_1 (N/mm ²)	γ_1	C_2 (N/mm ²)	γ_2
363.3	21	1.2	7993	175	6773	116
240	43	2.6	14202	320	12300	215

The parameters of the mentioned constitutive model are σ_0 , Q_∞ , b, C_i , γ_i . σ_0 is the yield stress at zero plastic strain; C_i and γ_i are the kinematic hardening parameters; Q_∞ and b are the isotropic hardening parameters. These parameters can be obtained by data fitting. The bond between steel reinforcement and concrete is assumed as a perfect bond, where the reinforcements are constrained in the concrete by using embedded region constraint, which allows each reinforcement element node to connect properly to the nearest concrete node. This type of bonding does not include the slip effects of reinforcements from concrete.

3.1.2 Applied loads

The specimen was subjected to unidirectional cyclic lateral loading under 40 kN constant axial loads, representing 10% of the column’s axial load bearing capacity, applied on each column. The lateral loading sequence is shown in Fig. 4 was a displacement-controlled type of loading scheme.

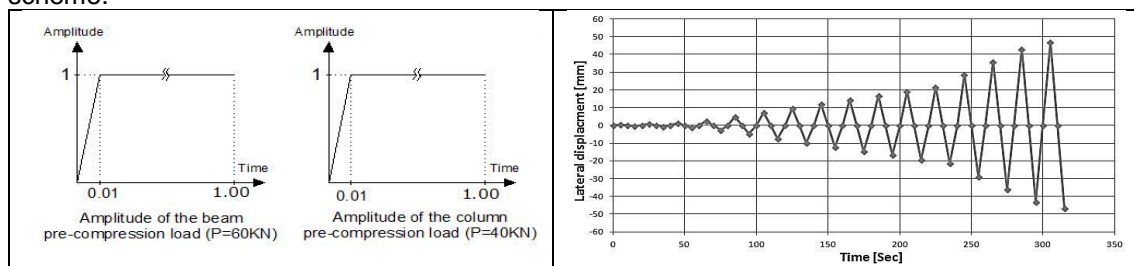


Fig. 4: The displacement-based loading protocol used in the tests Sakr et al. [13].

3.1.3 Comparison of experimental and finite element results

Fig. 4 illustrates a comparison between lateral load versus displacement curves of the bare frame predicted by the adopted numerical model and the experimental results. The figure clearly shows that the adopted numerical model was accurate in estimating the ultimate load carrying capacity of the bare frame.

The analysis reveals that the initial stiffness of the experimental response was very close to the initial stiffness of the adopted FE model. Therefore, the stiffness of the adopted model at intermediate loadings varied considerably from the experimental results; this is mainly due to the lack of the softening effect in the FE model of the concrete elements.

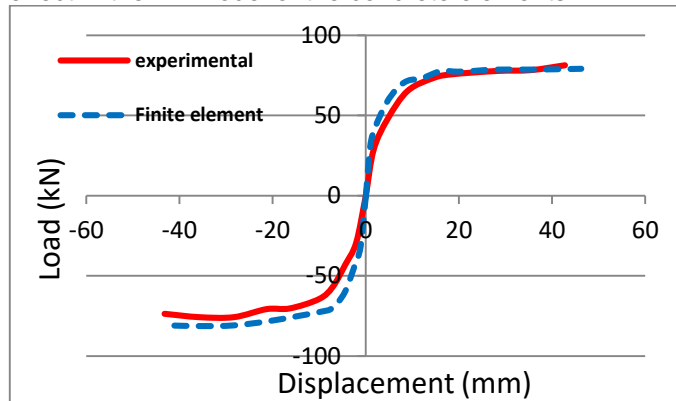


Fig. 5: Load –displacement curve (envelope of hysteretic curves) for bare frame.

Simulated failure mode is shown in Fig. 6. It is clear from the figure that, with increasing the applied load, the specimen failed due to the occurrence of plastic hinges forming at the same places in the experimental. It is clear from the above comparisons that the FE model (**2D plane stress element**) can simulate, with acceptable accuracy, the cyclic behavior of bare RC frame.

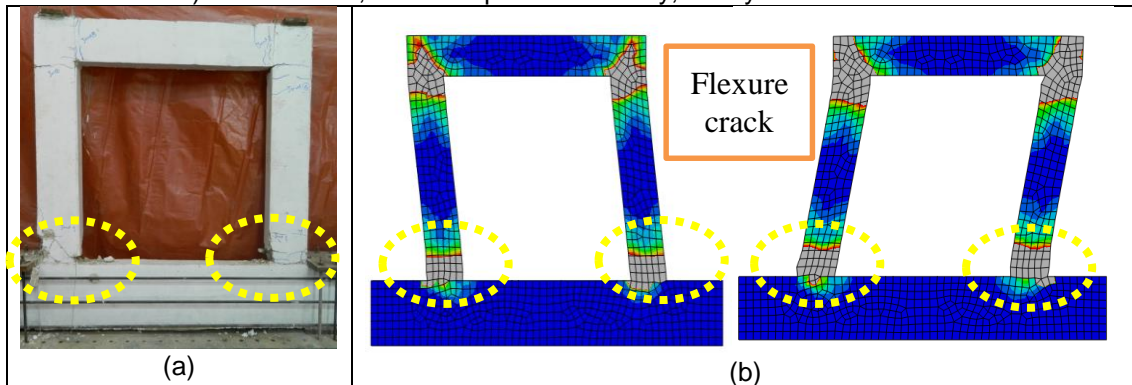


Fig. 6: Modes of failure and crack survey- (a)Damage pattern for BF (Experimental) – (b) plastic strain pattern cracks (2D Plane stress model).

3.2 Infilled frame

To calibrate the behavior of the infilled frame model, a comparison is carried out between the finite element results and that reported in the experimental work of Kyriakides et al. [16]. The experimental program consisted of $\frac{1}{5}$ scale model of a single-story concrete subjected to in-plane quasi-static cyclic tests. The concrete masonry unit (CMU) infill panel had a slenderness ratio (h/t) of 9.57. The specimen had an aspect ratio (h/w) of 0.56. Note that there are no stirrups in the upper beam. Dimensions and RFT details of the frame is shown in Fig. 7.

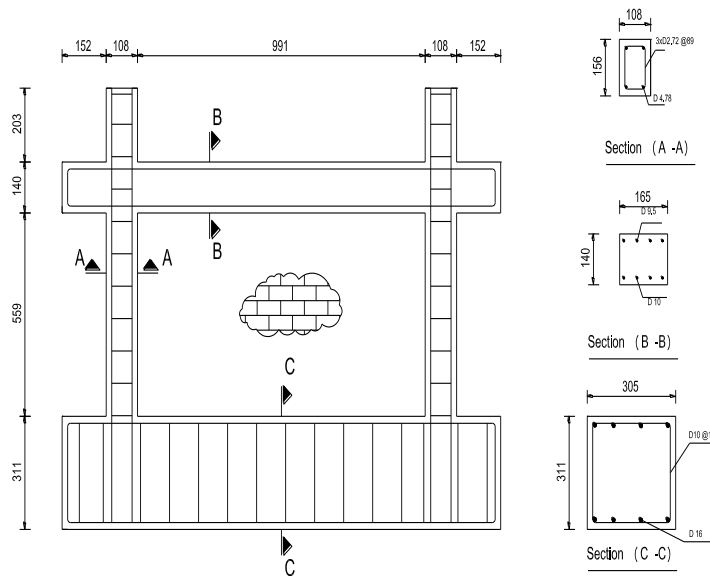


Fig. 7: Dimensions and reinforcement details of test frame Kyriakides et al. [16].

3.2.1 Material properties

3.2.1.1 Concrete

In the experimental study, the average compressive strength $\bar{\sigma}_c$ was in the experimental work 26.54 MPa, So the mechanical properties of the concrete were assumed the same that used in section (3.1.1.1).

3.2.1.2 Reinforcement steel

The properties for the steel reinforcements are shown in Table 2. A Poisson’s ratio of 0.3 was used for the steel reinforcement. full bond between steel reinforcement and concrete is assumed.

Table 2: Calibration parameters of steel

Type and Diameter (mm)	Yield stress (MP _a)	E (GPa)
Column transverse reinforcement (2.69)	228	206
Column longitudinal reinforcement (4.78)	772	260
Upper Beam longitudinal reinforcement (10)	372	206
Lower Beam longitudinal reinforcement (16)	372	206

3.2.1.3 Infill panel

The infill panel was represented as isotropic material. A linear relationship is imposed with a crushing plateau and tension cutoff point [18]. Hence a "damage plasticity model" is used to model the infill panel. Tensile strength for the concrete masonry used in the referenced experimental work was not provided, and as it is usually a parameter subjected to relatively high uncertainty , a conservative failure value of 2.50 N/mm² for tensile cracking was assumed according to [18]. The average compressive strength of the panel to represent it as isotropic material was assumed to be 23.14 MPa and the Elastic modulus was taken 16500 MPa according to [16]. To specify the post-peak tension failure behavior of concrete masonry, the fracture energy method is used. The fracture energy, G_f , is the area under the softening curve; It can be observed that the optimum value was found to be equal 348 J/m² [14] as a fraction of the concrete tensile fracture energy.

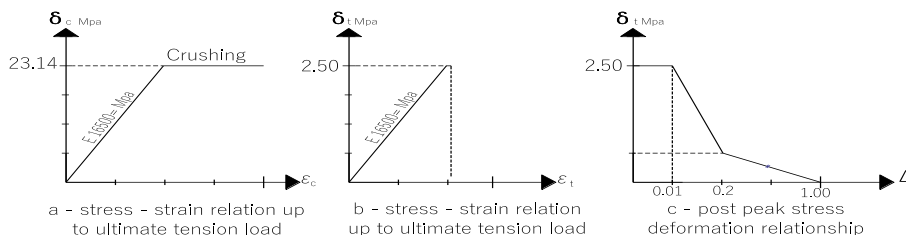


Fig. 8: Stress-strain relationships for infill panel

3.2.2 Applied loads

In the experimental work, the specimen was subjected to unidirectional cyclic lateral loading under 38.4 kN constant axial load applied on each column. Fig. 9(a) shows the loading protocol for the cyclic quasi-static test of specimen. The specimen was initially subjected to four cycles with the actuator moving under load control, two cycles up to 22.2 kN and two up to 44.5 kN. Then the procedure was switched to displacement control, subjecting the specimen to two cycles per drift level as shown in Fig. 9(b).

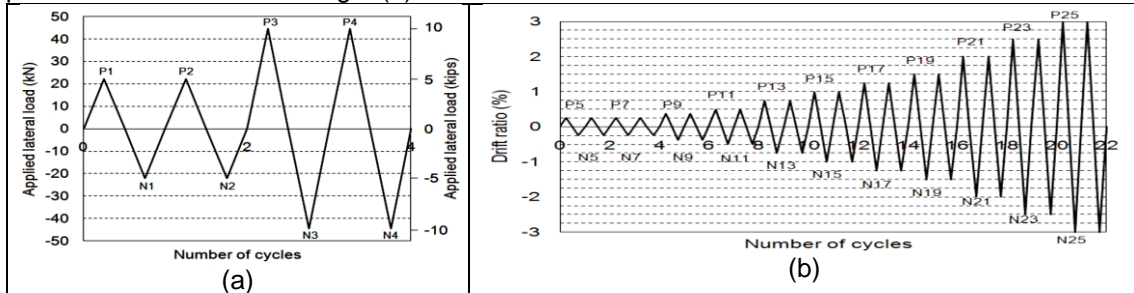


Fig. 9: (a) Load control- (b) Displacement control

3.2.3 Comparison of experimental and finite element results

Fig. 10, shows the hysteretic curve of lateral load versus drift ratio of the Infilled frame predicted by the adopted numerical model and the experimental results. Moreover, Fig. 11, illustrates a comparison between envelopes of lateral load versus displacement relationships of the infilled frame predicted by the adopted numerical model and the experimental results of Kyriakides [16]. It is shown that the FE analysis predicted the peak load quite accurately. The initial stiffness of the infilled frame in the FE model was somewhat higher than that predicted by the experimental result. However, the stiffness of the experimental and numerical infilled frame model gradually became closer as the load increased.

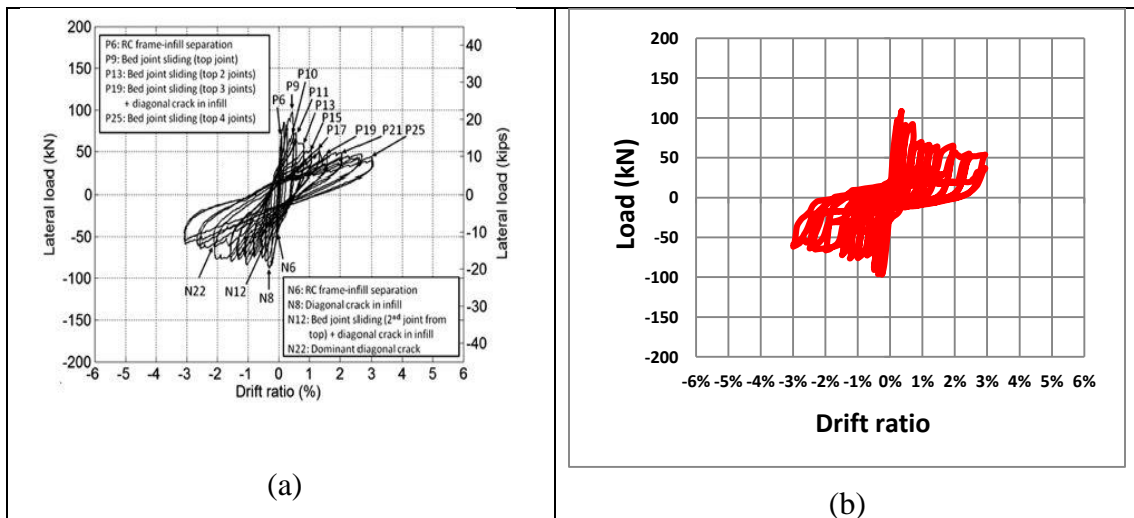


Fig. 10: Load versus drift ratio response: (a) The hysteretic curves for Experimental [16] - (b) The hysteretic curves for FE model (current study).

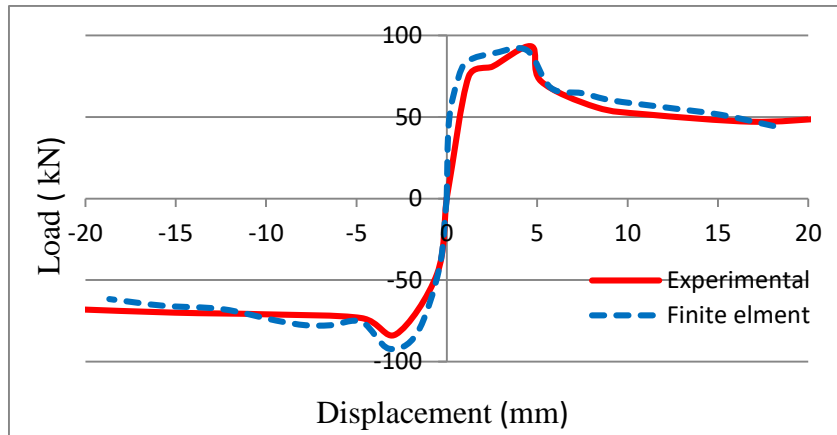


Fig. 11: Load –displacement curve (envelope of hysteretic curves) for infilled frame.

Fig. 12, illustrates a simulated failure mode of the infilled frame at 0.25% drift ratio, full separation of the masonry infill from the bounding concrete frame was observed. At the same drift level, the flexural crack formed in the column. It is clear from the above comparisons that the FE model (2D plane stress element) could simulate, with acceptable accuracy, the cyclic behavior of Infilled RC frame.

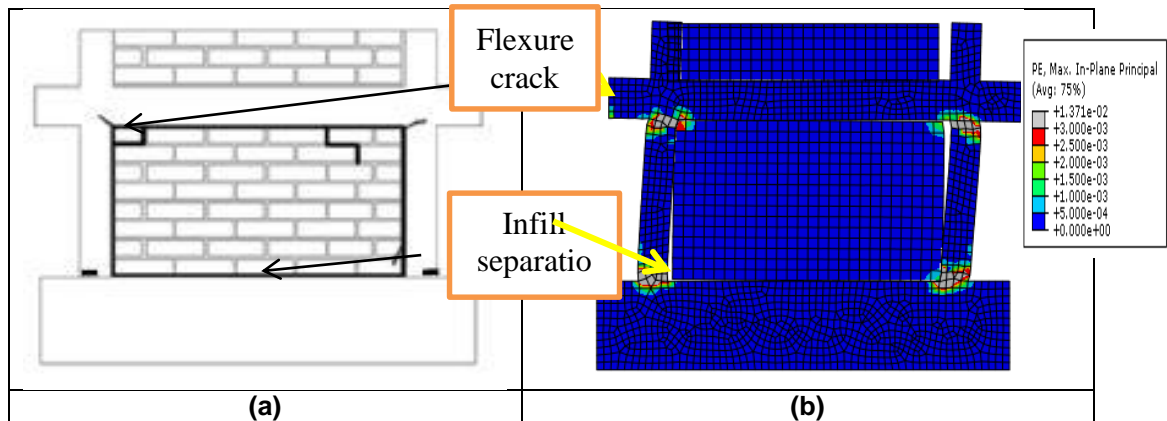


Fig. 12 Modes of failure and crack survey- (a) Damage pattern for infilled frame (Experimental[95]) - (b) Plastic strain pattern represents cracks (2D Plane stress model) at 0.25% drift ratio.

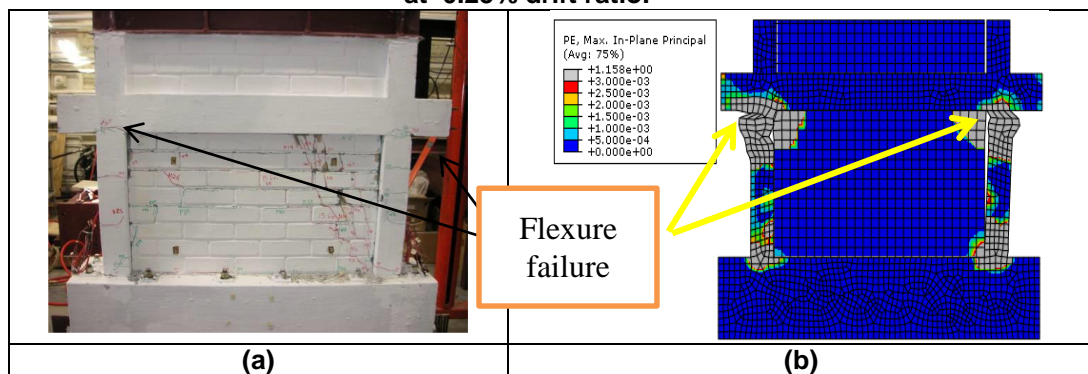


Fig. 13 Modes of failure and crack survey- (a) Damage pattern for infilled frame (Experimental[95]) - (b) Plastic strain pattern represents cracks (2D Plane stress model) at the end of the test.

3.3 Infilled frame retrofitted with 0.25% Reinforcement ECC

To calibrate the behavior of the infilled frame model retrofitted with ECC, a comparison is carried out between the finite element results and that reported in the experimental work of Kyriakides et al. [16], Dimensions and RFT details of the frame is shown in Fig. 6. The ECC layer was applied to one side and it was 12.7mm thick and reinforced with welded wire fabric (WWF) comprising 0.25% of the cross section of the ECC.

3.3.1 Material properties

The mechanical properties of the concrete, the infill panel and the Reinforcement steel were the same that used in section (Error! Reference source not found.).

3.3.1.1 ECC material

As described before, the CDP criterion is used to model the ECC. The compressive behavior of ECC was obtained based on the experimental work [16]. The average compressive strength of 59 MPa at a strain level of 0.55% as shown. The stress–strain relationship in compression for concrete is represented in Fig. 14. Poisson’s ratio was assumed to be 0.2. To specify the post-peak tension failure behavior of ECC the fracture energy method was used. The fracture energy for mode I, G_f , is the area under the softening curve. Many trials have been carried out to find the optimum value of fracture energy and compared with other values that available in the literature to determine it and was found to be equal 3000J/m² [19].

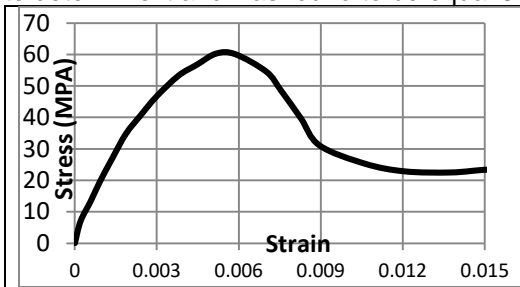


Fig. 14 Stress–strain relationship under uni-axial compression [M].

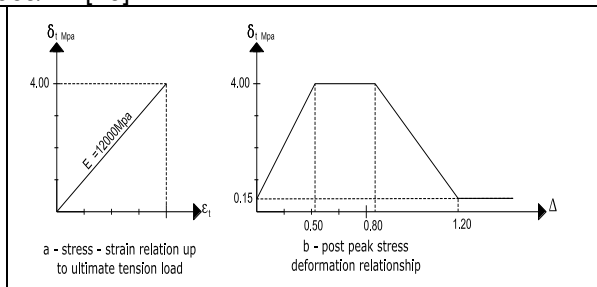


Fig. 15 ECC stress strain relationship under uniaxial tension

3.3.1.2 WWF steel reinforcement

The properties for the WWF steel reinforcements show in Table 3. A Poisson’s ratio of 0.3 was used for the WWF steel reinforcement. A fully bonded between WWF and ECC material.

Table 3: The properties of WWF steel reinforcements

Type and Diameter (mm)	Yield stress (MPa)	E (GPa)
WWF reinforcement (1.6)	372	151.5

3.3.2 Contact modeling

3.3.2.1 ECC- infill wall interface

For 2D model using shell element, the adhesive layer was modeled using cohesive node-to-node interaction model. Fig. 1, shows a graphic interpretation of a simple bilinear traction–separation law written in terms of the effective traction τ and effective opening displacement δ . The interface is modelled as a rich zone of small thickness.

The values used for this study were $K_{nn}=88500 \text{ N/mm}^3$ and $K_{tt}=15450 \text{ N/mm}^3$ [20]. The maximum shear stress, τ_{max} was taken 1.2 MPa and the tensile strength bond σ_{max} was taken 0.7 MPa [20]. For the fracture energy, G_{cr} in the two shear directions, many trials have been carried out to find the optimum value and were found to be equal 5000 J/m² shown good an agreement with the experimental results.

3.3.3 Applied loads

The applied loads were the same that used in section (3.2.2)

3.3.4 Comparison of experimental and finite element results

Fig. 16, shows the hysteretic curve of lateral load versus drift ratio of the Infilled frame retrofitted with ECC predicted by the adopted numerical model and the experimental results. Moreover, **Error! Reference source not found.** 17, illustrates a comparison between envelopes of lateral load versus displacement relationships of the Infilled frame retrofitted with ECC predicted by the adopted numerical model and the experimental results of Kyriakides [16]. At approximately 7 mm, shear failure occurred at the top end of both columns, and from that point on the specimen maintained a lateral load capacity of approximately 75 kN. It is shown that the FE analysis predicted the peak load quite accurately, but at 1% drift ratio conversion in solution is occurred after shear failure.

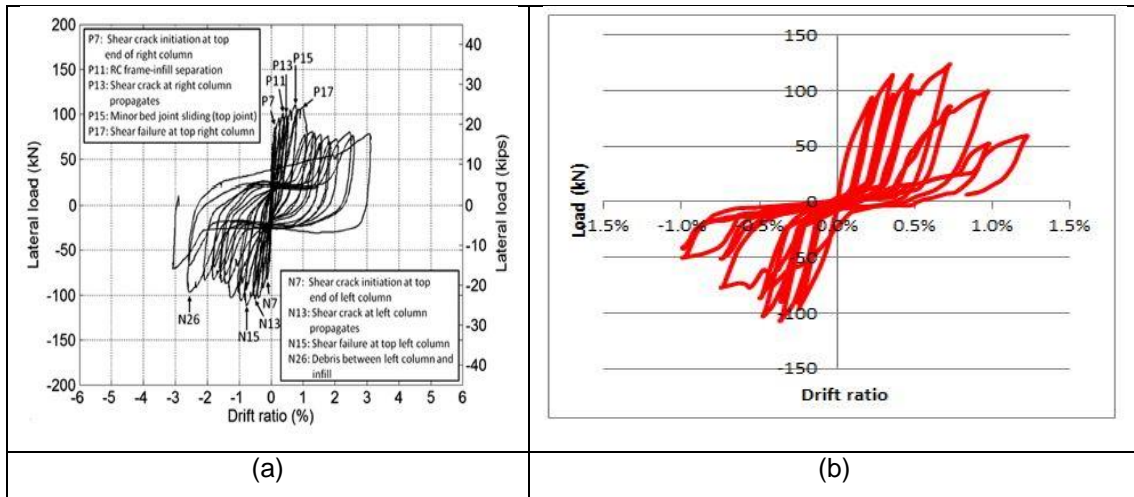


Fig. 16: Load versus drift ratio response: (a) The hysteretic curves for Experimental [16] - (b) The hysteretic curves for FE model (current study).

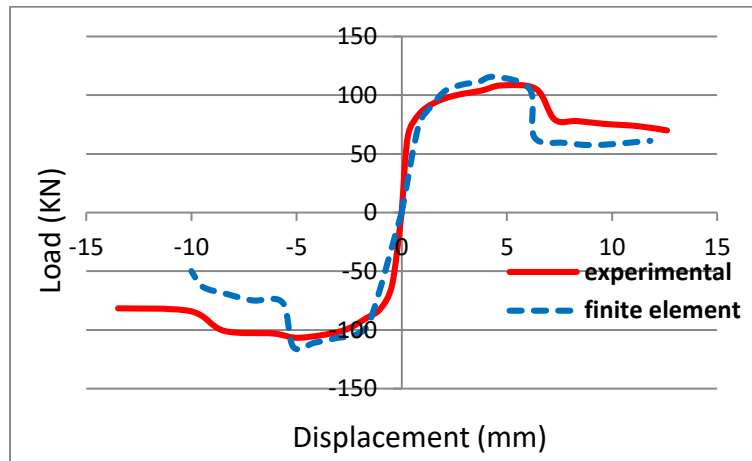


Fig. 17: Load –displacement curve (envelope of hysteretic curves) for infilled frame retrofitted with ECC.

Fig. 18, illustrates a simulated failure mode of the specimen at 0.5% drift ratio. At the same drift, the infill was fully separated from the bounding frame and the shear cracks at the beam-column joints propagated. The flexural cracks at the upper end of both columns became wider and large tensile cracks formed at the base of the columns that agreed with the strain gauge readings. It is clear from the above comparisons that the FE model (**2D plane stress element**) can simulate, with acceptable accuracy, the cyclic behavior of Infilled RC frame.

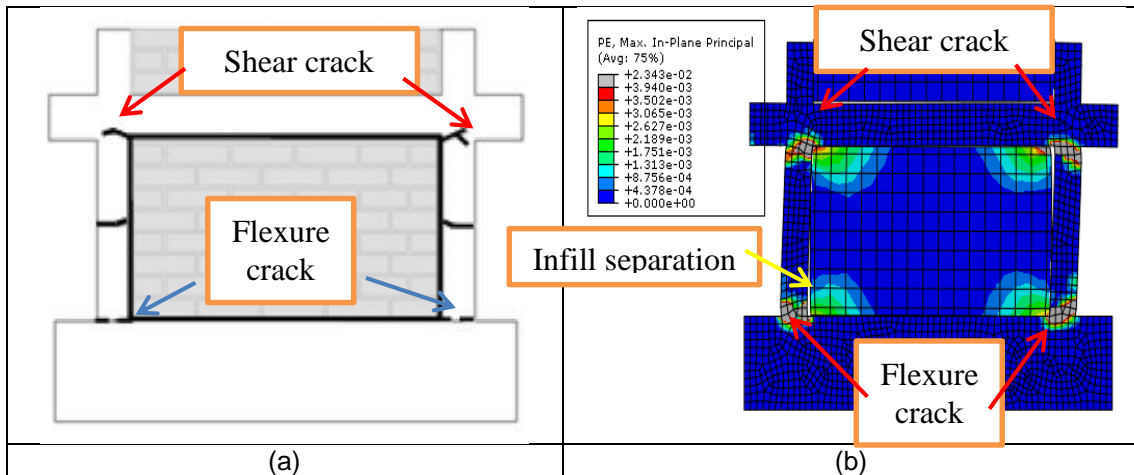


Fig. 18: Modes of failure and crack survey- (a) Damage pattern for infilled frame(Experimental[K]) (b) Plastic strain pattern represents cracks (2D Plane stress model) at 0.5% drift ratio .

4. PARAMETRIC ANALYSIS

4.1 Column depth with different type of infill panel

After the calibration of the numerical model, it was decided to make a parametric analysis to investigate the effect of RC column depth (column shear strength) on the behavior infilled frame, so two specimens with different column depth of 400 and 600 mm with the same width 200 mm and with the same reinforcement details are presented as shown in Fig. 19. The main reason to have different column depth is that the mode of failure in infilled frames can be changed from ductile failure (four plastic hinge of column) to brittle failure (column – shear failure) in one specific story, where the mode of failure of full-scale infilled frame must be known to be retrofitted by ECC material with suitable strategy. Symbolic meaning and configuration of the different parameters are summarised in Table 4.

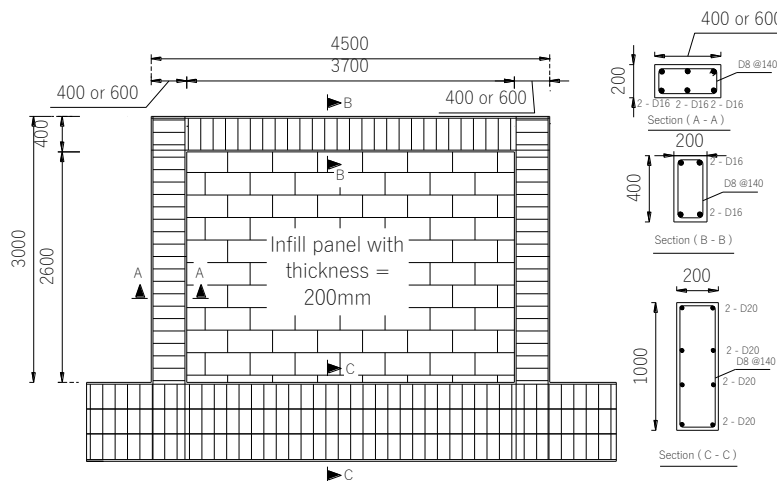


Fig. 18:Dimensions and RFT details for specimens

Table 0: Symbolic meaning of different parameters

No	Symbol	Column depth	Infill panel properties		Details of frame
			σ_c (MPa)	σ_t (MPa)	
1	SI	600	4.8	0.65	Strong Infilled
2	SI*	400	4.8	0.65	Strong Infilled
3	WI	600	1.8	0.22	Weak Infilled
4	WI*	400	1.8	0.22	Weak Infilled

To represent the infill panel as isotropic material, A comparison of the behaviors of frames infilled with weak infill panels (with compressive strength = 1.8 N/mm² and tensile strength = 0.22 N/mm²) [22] and frames infilled with strong infill panels (with compressive strength = 4.80 N/mm² and tensile strength = 0.65 N/mm²) [21] is presented as shown in Fig. 20 and Fig. 21. The main reason to have different type of infill is that the improvement of the lateral strength, initial stiffness and cumulative dissipated energy of the masonry infilled RC frame by increasing the compressive strength of masonry is much associated to the crack patterns and damage developed in the composite structure. In fact, the damage pattern is much related to the crushing of masonry at the ends of the compression strut at the contact between the masonry infill and the frame and the mode of failure can be changed from brittle failure to ductile failure, so that it must be known the mode of failure of infilled frame.

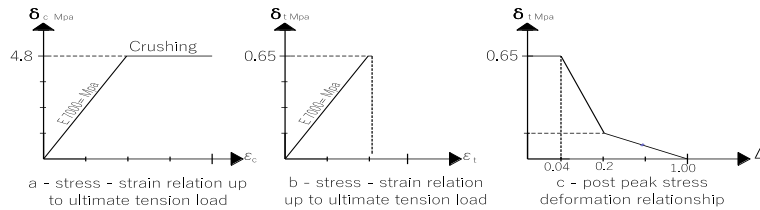


Fig. 19: Stress–strain relationships for strong infill panel

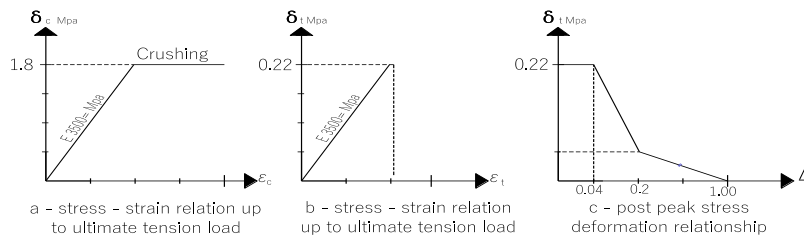


Fig. 20: Stress–strain relationships for weak infill panel

Fig. 21, shows the hysteretic curves of specimens for infilled frames. The peak load and corresponding displacement are 471 kN at 5 mm for specimen SI, and 371 kN at 2.33 mm for specimen SI* followed by a drop in its load carrying capacity to lateral load of 257 at 5.9 mm, because the brittle shear failure is occurred at the tip of the column in push direction. For specimen SI a gradual reduction in the strength of specimen SI occurred with the increase in the imposed displacements after the maximum strength was attained. For infilled frame with weak brick the pinching effect somewhat is less than that of infilled frame with strong brick due to the occurrence of plastic hinges forming and diagonal crack in the infill panel

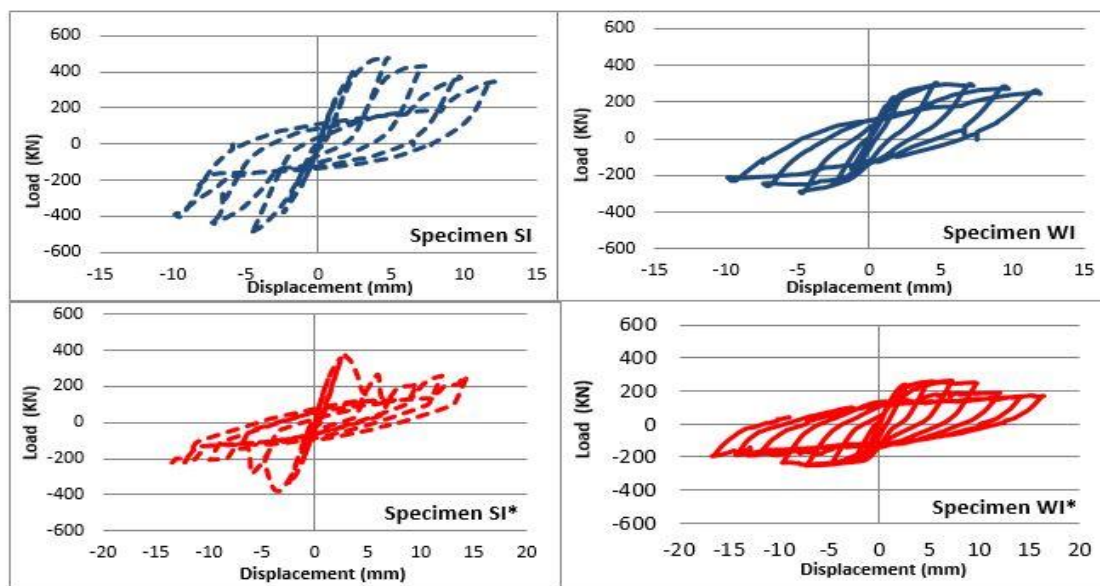


Fig 21: The hysteretic curves of specimens for different type of infilled frame

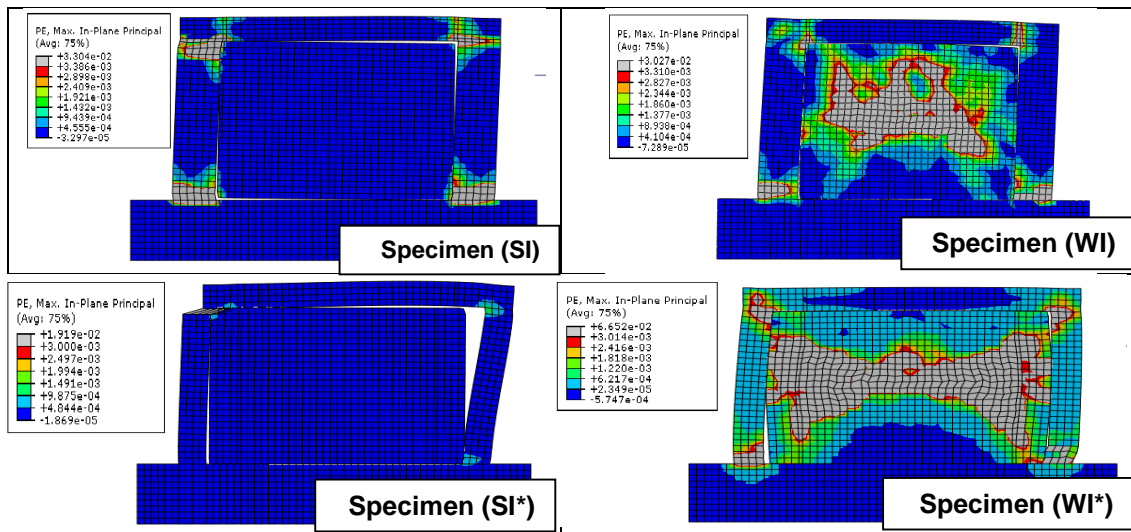


Fig. 22: Plastic strain of specimens at Maximum Load.

Another interpretation of results is listed in Table 5. This table indicates the ultimate load, the failure mode that occurred at maximum load. Where d_{pu} represents that the displacement at the ultimate load

Table 5: Numerical results and characteristics specimens

Specimen	P_u (kN)	d_{pu} (mm)	Failure mode
SI	471	4.6	Column plastic hinge
WI	325	2.8	Column plastic hinge and diagonal crack in the infill panel
SI*	371	2	Column shear
WI*	259	5	Column plastic hinge and diagonal crack in the infill panel

4.2 ECC retrofitting configuration

To the authors' knowledge, this study aims to investigate different retrofitted configuration by using the ECC layer on RC frame only or infill panel only or both, the infilled frame is retrofitted with 2 cm ECC layers on both sides. So that, the purpose of this study is to choose the best retrofitted configuration by using the ECC layer on infill panel only or RC frame only or whole.

4.2.1 Contact modelling

The contact modelling between the infill wall-ECC interface is the same that used in section (Error! Reference source not found.).

4.2.1.1 Infill wall-concrete interface

For 2D model using shell element, the adhesive layer was modeled using cohesive node-to-node interaction model. Fig. 1 shows a graphic interpretation of a simple bilinear traction–separation law written in terms of the effective traction τ and effective opening displacement δ . The interface is modelled as a rich zone of small thickness. The values used for this study are $K_{nn}=88500 \text{ N/mm}^3$ and $K_{tt}=15450 \text{ N/mm}^3$ [20].The maximum shear stress, τ_{max} was taken 1.2 MPa and the tensile strength bond σ_{max} was taken 0.7 Mpa [20]. The value of the fracture energy used in all next specimens is constant and equal to 5000J/m.

4.2.1.2 ECC-ECC interface

A surface-to-surface contact definition is used to model contact interactions between the ECC at the surface that infill panel contact with concrete frame interior surface and the infill panel. The values used for this study were $K_{nn}= 4425 \text{ N/mm}^3$ and $K_{tt}=1925 \text{ N/mm}^3$. The maximum shear stress, τ_{max} is taken 1.5 MPa and the tensile strength bond σ_{max} was taken 5 MPa [20]. The value of the adhesive layer fracture energy used in all next specimens is constant and equal to 4500J/m.

4.2.2 Results

Error! Reference source not found. 23, shows the envelop of hysteretic curves of specimens for different retrofitted configurations.

For retrofitted Specimen **SI**, it is noted that, the specimen (**RB-SI-T2**) have little increase in the ultimate load by 2% because there is shear failure at the tip of the columns. The ultimate load by the specimen (**RA-SI-T2**) is found to be 652 KN which exhibited a 40 % increase to that of unreinforced specimen SI.

For retrofitted Specimen **WI**, the specimen (**RC-WI-T2**) have little increase in the ultimate load by 6% due to bed joint sliding and a diagonal crack in the masonry infill occurred, forming a knee braced mechanism. The additional ECC on both RC-frame and brick has a great effect on the retrofitted frame response.

For retrofitted Specimen **SI***, it's clear that the specimens (**RB-SI-T2**) and (**RC-SI*-T2**) have little increase in the ultimate load by 6% and 2% because there is shear failure at the tip of the columns.

For retrofitted Specimen **WI***, the specimens (**RC-WI*-T2**) has little increase in the ultimate load by 4% because there is shear failure at the tip of the columns. The additional ECC on brick only or both RC-frame and brick has a great effect on the retrofitted frame response. Although specimens (RC-SI-T2) is retain their carrying their ultimate capacity up to 15 mm displacement due to ductile failure.

It's clear that, the additional ECC on both RC-frame and brick has a great effect on the retrofitted frame response for all infilled frame specimens.

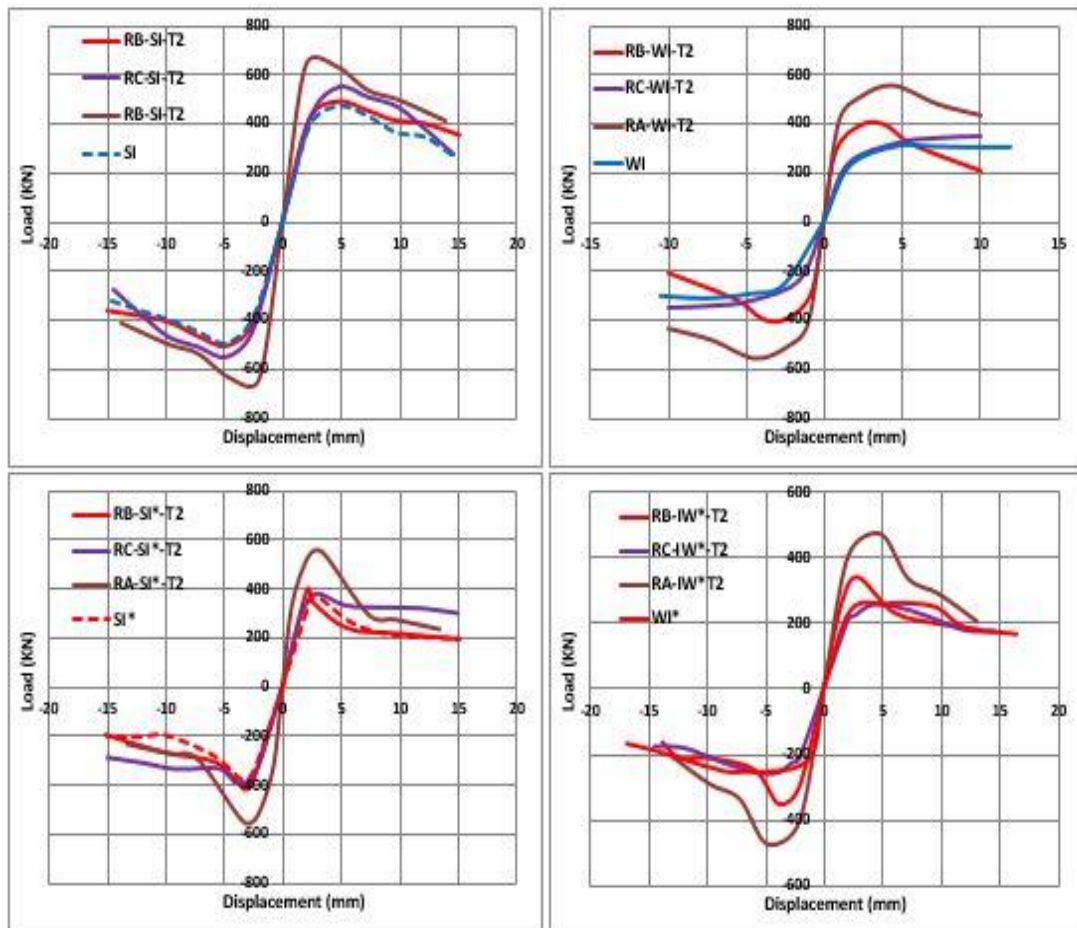


Fig. 23: Load –displacement curve (envelope of hysteretic curves) for different retrofitted configurations of specimens.

Another interpretation of results is listed in Table 6. This table indicates the ultimate load, the failure mode that occurred at maximum load.

Table 6: Numerical results and characteristics specimens

Specimen	P_u (kN)	d_{pu} (mm)	Failure mode	P_u/P_{uWI}
SI	465	5	Column plastic hinge	1
RB-SI-T2	471	4.7	Column shear and plastic hinge	1.02
RC-SI-T2	548	4.7	Column plastic hinge	1.18
RA-SI-T2	652	2.5	Column plastic hinge	1.40
WI	325	5	Column plastic hinge and diagonal crack in the infill panel	1
RB-WI-T2	396	4.8	Column shear and plastic hinge	1.22
RC-WI-T2	346	5	Column plastic hinge and diagonal crack in the infill panel	1.06
RA-WI-T2	556	2.25	Column plastic hinge	1.71
SI*	371	2.6	Column shear	1
RB-SI*-T2	394	2.2	Column shear	1.06
RC-SI*-T2	379	3.4	Column plastic hinge	1.02
RA-SI*-T2	544	3.2	Column shear and plastic hinge	1.46
WI*	259	4.6	Column plastic hinge and diagonal crack in the infill panel	1
RB-WI*-T2	328	2.8	Column shear	1.27
RC-WI*-T2	270	5	Column plastic hinge and diagonal crack in the infill panel	1.04
RA-WI*-T2	474	4.8	Column plastic hinge	1.83

Where d_{pu} represents that the displacement at the ultimate load and P_u/P_{uWI} represents the ratio of the ultimate load of specimen and the ultimate load of specimens.

5. CONCOULSION

Based on the results presented in this study, the following conclusions can be drawn:

1. Results indicated that 2D model using plane stress element was able to predict the actual behavior of the bare frame, infilled RC frame and infilled RC frames retrofitted with ECC efficiently.
2. The increase in column's depth significantly increase the lateral strength, initial stiffness for infilled frame.
3. By increasing infill's compressive strength from 1.8 MPa to 4.8MPa, infilled frame's lateral strength increased about 45% for the various depth of the column respectively.
4. Specimen SI shows the highest ultimate capacity and initial stiffness. On contrary, the specimen WI* has the lowest ultimate capacity and initial stiffness.
5. All infilled frames have a ductile failure except in the specimen SI* where has a brittle failure (shear failure).
6. The mode of failure in infilled frames can be occurred in RC-frames or infill panel and may be changed from ductile failure (four plastic hinge of column) to brittle failure (column – shear failure) in one specific story, so that the mode of failure of full-scale infilled frame must be known to be retrofitted by ECC material with suitable strategy.
7. If only the brick is retrofitted, all the specimens can be observed that increase the stiffness of the wall, this is leading to brittle failure and shear failure occurred.
8. The optimum retrofitted configuration to infilled RC- framed is that applying the ECC material on both RC-frame and brick together, it has a great effect on the lateral strength, initial stiffness and cumulative dissipated energy for the retrofitted infilled frame response

REFERENCE

1. Franklin, S., J. Lynch, and D. Abrams. (2001), "Performance of Rehabilitated URM Shear Walls: Flexural Behavior of Piers", Department of Civil Engineering, University of Illinois at Urbana-Champaign, Urbana, Illinois.
2. ElGawady, M.A., P. Lestuzzi, and M. Badoux. (2006), "Shear Strength of URM Walls Upgraded with FRP", Engineering Structures, p. 1343- 1352.

3. Taghdi, M., M. Bruneau, and M. Saatcioglu. (2000), "Retrofitting of Low-Rise Masonry and Concrete Walls Using Steel Strips", *ASCE Journal of Structural Engineering*, p. 1017-1025.
4. El-Dakhakhni, W.W., A.A. Hamid, and M.F. Elgaaly. (2004), "Seismic Retrofit of Concrete-Masonry-Infilled Steel Frames with Glass Fiber-Reinforced Polymer Laminates", *ASCE Journal of Structural Engineering*, p. 1343-1352.
5. Mander, J.B. (1993), "An Experimental Study on the Seismic Performance of Brick-Infilled Steel Frames with and Without Retrofit", Technical Report No. NCEER-93-0001, National Center for Earthquake Engineering Research, State University of New York, Buffalo, NY.
6. Li, V.C. and C.K.Y. Leung. (1992), "Steady state and multiple cracking of short random fiber composites", *ASCE J. of Engineering Mechanics*, p. 2246-2264.
7. Kim, Y.Y., G. Fischer, and V.C. Li. (2004), "Performance of bridge deck link slabs designed with ductile ECC", *ACI Structural*, p. 792-801.
8. Bertero, V.V. and S. Brokken. (1983), "Infills in Seismic Resistant Building", *ASCE Journal of Structural Engineering*, p. 1337-1361.
9. Mehrabi, A.B. (1994), "Performance of Masonry-Infilled R/C Frames under In-Plane Lateral Loads", Report No. CU/SR-235 94-6, Dept. of Civil, Environmental, and Architectural Engineering, University of Colorado, Boulder, CO.
10. Mehrabi, A.B. (1996), "Experimental Evaluation of Masonry-Infilled RC Frames", *ASCE Journal of Structural Engineering*, p. 228-237.
11. A.A. T. and M. A. (2011), "Investigation on the behavior of brick-infilled steel frames with openings, experimental and analytical approaches", *Engineering Structures*, p. 968-980.
12. ABAQUS, Analysis User's Manual. Version 6.12, ABAQUS, Inc., Dassault Systemes, USA.
13. M. A. Sakr, S. R. El-khoriby, A. A. Seleemah, and M.M. Aboelnour, (2017), " Experimental and numerical study on masonry Infilled rc frames under cyclic loads", *International Conference on Advances in Structural and Geotechnical Engineering*.
14. Mohamed A. Sakr, Saher R. El-khoriby, Ayman A. Seleemah, and Essam A. Darwish, (2015), " Numerical Modeling of Infilled RC Frames Using Three Different Models", *International Conference on Advances in Structural and Geotechnical Engineering*.
15. Saenz L, S., Discussion of "Equation for the stress-strain curve of concrete", *ACI Journal*, 1964.
16. M.A. Kyriakides, and S.L. Billington, (2014) "Cyclic Response of Nonductile Reinforced Concrete Frames with Unreinforced Masonry Infills Retrofitted with Engineered Cementitious Composites", *American Society of Civil Engineers*.
17. M. Wang, Y. Shi, Y. Wang, G. Shi, (2013) "Numerical study on seismic behaviors of steel frame endplate connections", *J. Constr. Steel Res.* 90 P. 140–152.
18. D'Ayala D., Worth J., and Riddle O., (2009) "Realistic shear capacity assessment of infill frames: Comparison of two numerical procedures". *Engineering Structures*, 31(8): p. 1745-1761
19. Mahmud, G.H., Z. Yang, and A.M.T. Hassan, Experimental and numerical studies of size effects of Ultra High-Performance Steel Fibre Reinforced Concrete (UHPFRC) beams. *Construction and Building Materials* 2013: p. 1027–1034.
20. Kyriakides, M., SEISMIC RETROFIT OF UNREINFORCED MASONRY INFILLS IN NON-DUCTILE REINFORCED CONCRETE FRAMES USING ENGINEERED CEMENTITIOUS COMPOSITES. PHD at Stanford University, 2011.
21. Mohamed A. Sakr, Saher R. El-khoriby, Ayman A. Seleemah and Essam A. Darwish, " Behavior of CFRP Retrofitted Infilled RC Frame: Finite Element model" *Proc. Of the second intel. Conf. on advances in civil, structural and Mechanical engineering – CSM 2014*. ISBN: 978-1-63248-054-5 doi: 10.15224/ 978-1-63248-054-5-100
22. Markulak, D., I. Radić, and V. Sigmund, Cyclic testing of single bay steel frames with various types of masonry infill. *Engineering Structures*, 2013: p. 267-277.
23. A, F., N. A, and M. P. (2012), "The influence of masonry infill on the seismic behaviour of RC frame buildings", *Engineering Structures*.
24. Obaidat, Y.T., S. Heyden, and O. Dahlblom. (2010), "The effect of CFRP and CFRP/concrete interface models when modelling retrofitted RC beams with FEM", *Composite Structures*.